Tellus (1996), 48B, 347–360
Printed in UK – all rights reserved

TELLUS
ISSN 0280–6509

The effect of hygroscopicity on cloud droplet formation

By MARKKU KULMALA[1], PEKKA KORHONEN*, TIMO VESALA, HANS-CHRISTEN HANSSON†, KEVIN NOONE† and BIRGITTA SVENNINGSSON‡, *University of Helsinki, Department of Physics, P.O. Box 9 (Siltavuorenpenger 20D), FIN-00014 University of Helsinki, Finland; *Finnish Meteorological Institute, Air Quality Department, Sahaajankatu 22 E, SF-00810 Helsinki, Finland; †Stockholm University, Department of Meteorology, S-10691 Stockholm, Sweden; ‡University of Lund, Department of Nuclear Physics, Sölvegatan 14, S-22362 Lund, Sweden*

(Manuscript received 8 May 1995; in final form 8 November 1995)

ABSTRACT

The effects of particle hygroscopicity and the availability of condensable material (other than water) in the gas phase on cloud droplet formation and the radiative properties of clouds have been studied using an adiabatic air parcel model with detailed multicomponent condensation. The pre-existing log-normal particle distribution used is bimodal in size and bimodal in hygroscopicity. To simulate this, four log-normal distributions were used and in each mode particles were assumed to be internally mixed, i.e., they are composed partly of salt and partly of an insoluble substance. The mean diameters, standard deviations, total number of pre-existing particles, the mass fraction of the soluble salt and initial concentration of condensable vapour were varied in the simulations. There is a clear effect of hygroscopicity on the activated fraction of aerosol particles in our simulations. Thus hygroscopicity of pre-existing aerosol particles and concentrations of condensable gases can also influence the optical thickness and reflectance of clouds. The change in optical thickness varies as a function of the number concentration of pre-existing particles, having a maximum ($\Delta\tau/\tau = 0.2$) near a concentration of 1000/cc.

1. Introduction

The increased concentration of greenhouse gases (e.g., carbon dioxide, methane) can have large effects on the earth's climate by possibly increasing the greenhouse effect. However, much attention has recently been given to the possibility that the increased concentrations of aerosol particles can have a direct and an indirect (via clouds) tendency to cool the earth's surface (Charlson et al., 1991; Charlson et al., 1992; Charlson and Wigley, 1994).

Clouds have major effects on the scattering and absorption of electromagnetic radiation in the Earth's atmosphere. Locally the net effect is not so evident (e.g., because of different kind of surfaces) (Curry, 1995). But according to measurements, the global net effect of today's polluted clouds on the climate is probably cooling (Hartmann and Doelling, 1991) and thus opposite to the effect of greenhouse gases. The optical properties of clouds depend on their depth, liquid water content and cloud droplet size distribution (Twomey, 1977).

The formation and growth of cloud droplets occur on pre-existing aerosol particles. The pre-existing particle distribution strongly effects the developing cloud droplet distribution. According to our recent simulations the soluble mass of pre-existing aerosol particles is the most important factor (other than dynamics) influencing the activation process (Korhonen et al., 1994). This is because hygroscopic material lowers the saturation vapour pressure of water vapour above the

* Corresponding author.

surface of a solution droplet and makes the formation of a cloud droplet easier. Field experiments show that the pre-existing aerosol particle distribution is usually composed of mixed particles, i.e. particles include both hygroscopic and insoluble components (Zhang et al., 1993; Svenningsson et al., 1992, 1994).

Recently, much attention has been given to the possibility that increasing number of sulfur compounds in the atmosphere could lead to an increase in the amount of sulfuric acid and ammonium sulfate particles. This could lead also to increased cloud droplet concentrations (Charlson et al. 1992; Charlson and Wigley, 1994). Kulmala et al. (1993, 1995), have studied an additional mechanism: that some other condensing gaseous pollutants (nitric acid in their case) could influence on the number of cloud droplets due to the increased amount of hygroscopic matter in the developing cloud droplets. Indeed, measurements show that there is close (albeit nonlinear) relationship between the cloud droplet size distribution and atmospheric pollutants (Leaitch et al., 1992). Some studies, based on satellite measurements, find higher albedos from the polluted areas of United States and Asia (Kim and Cess, 1993) as one could expect, while some other studies find no effects caused by changes in the albedo of the clouds in the northern hemisphere (Schwartz, 1988). Thus, it is evident that we do not sufficently understand the real effects of pollutants on the formation of cloud droplets, and on atmospheric radiation and climate.

The amount of water vapour available during the growth process is strongly dependent on various dynamical aspects and the particle size distribution. Particles carrying more hygroscopic material consume more water vapour during their growth before achieving the maximum saturation. The maximum saturation ratio reached is typically smaller in the case when we have more soluble material in the nascent droplets than in the case when we have less soluble material in the droplets. Thus it is not self-evident that the nascent cloud droplet distributions are much different in the cases of different initial amounts of hygroscopic material. On the other hand, condensation of some strongly hygroscopic gaseous substances on the particles simultaneously with water vapour can allow a larger fraction of the pre-existing particle distribution to grow to cloud droplets.

In this study we have investigated the effects of particle phase and gas phase hygroscopicity (the availability of condensable material in the gas phase) on the formation of cloud droplets in the situation where water (H_2O) and nitric acid (HNO_3) vapours are condensing on the mixed particles composed of ammonium nitrate (NH_4NO_3) and some insoluble substance. Nitric acid compounds were chosen due to increasing recognition of their importance (Kulmala et al., 1995). The pre-existing aerosol particle distribution is divided into two+two log-normal size distributions, to handle the bimodality in both size and hygroscopicity. In order to take into account the dynamical aspects, we have used an adiabatic air parcel model (Kulmala et al., 1993). The initial mean radii, standard deviations and number concentrations as well as the fraction of soluble salt in the particles and the concentration of gaseous HNO_3 in ambient air were varied. We have also investigated how the optical thickness of clouds will vary as a function of soluble mass fraction and initial nitric acid concentration.

2. Hygroscopic properties of atmospheric aerosols

The hygrocopic properties of atmospheric aerosols can be measured by determining their hygroscopic growth factor. The instrumentation used to determine the hygroscopic growth has typically been a Tandem Differential Mobility Analyser (TDMA) (Stolzenburg and McMurry, 1988; Svenningsson et al., 1992, 1994). A TDMA consists of 3 main parts.

The first differential mobility analyser (DMA) (with dry sheath air) is typically set to transmit a narrow particle size fraction, a quasi-monodisperse aerosol, selected from the ambient aerosol. This size can easily be selected in the size range 30–500 nm. After the first DMA the aerosol flow is split: part of it is directed to a Condensation Nucleus Counter to detect the total particle concentration in the selected particle size range. The other part is directed to a humidifier. In the aerosol humidifier the size of aerosol particles is increased at fixed relative humidity. The second DMA, with relative humidity controlled sheath air, and a CNC are used to detect the size of particles after hygroscopic growth in the humidi-

fier. A detailed description can be found in Svenningsson et al. (1992, 1994).

The hygroscopic growth for pure salt particles can be calculated from the water activity as a function of salt concentration, the Kelvin effect and the composition of the salt. If the mass fraction of the soluble material in the particles is less than unity, the hygroscopic growth factor is smaller. The mass fraction of soluble material can be determined comparing experimental growth factors with theoretical ones (Svenningsson et al., 1992, 1994).

In field experiments typically two distinct groups of particles with different hygroscopic growth have been seen (Hansson et al., 1994; Svenningsson et al., 1994). Actually these groups can be represented using log-normal distributions in the hygroscopic growth spectra. One group of particles were centered at about 5% growth in particle diameter and other were centered at about 40% growth in particle diameter at 85% relative humidity. The two groups were named less and more hygroscopic, respectively. Usually, the two hygroscopic groups were found in varying ratios, sometimes as a function of particle size. A rough estimate is that the fraction of less hygroscopic particles in background aerosol is 30% in number and mass (Hansson et al., 1994). Closer to anthropogenic sources and for smaller particle sizes (in Aitken mode) the fraction can reach considerably high values, such as 60% (Hansson et al., 1994). These results have given us input values for model calculations.

3. Formation and condensational growth of cloud droplets

In investigations of cloud microphycis using computer models, it is essential that the environment is described as realistically as possible. However, all cloud models involve some uncertainties. Since the aim of our studies is to investigate the effect of hygroscopicity on number concentration of cloud droplets we have used simple convection model to describe a rising air parcel (Pruppacher and Klett, 1978). The air parcel contains aerosol particles, water and some other condensable vapour (in this study nitric acid). We have assumed a constant updraft velocity without entrainment, since we are primarily interested in droplet formation, and entrainment starts to significantly influence the droplet size distribution only after the formation stage. The aerosol particles in the parcels are described using four log-normal size distributions. Typically, the first distribution consists of less hygroscopic Aitken mode particles, the second more hygroscopic Aitken mode particles, the third less hygroscopic accumulation mode particles and the fourth more hygroscopic accumulation mode particles. This is clarified in Fig. 1.

In the beginning of a simulation (below cloud base) particles take up water and acid from the gas phase until they reach equilibrium with their environment. The air parcel starts to rise and cool adiabatically and the saturation ratios of condensing vapours increase. Haze particles in the parcel take up more and more vapours and, depending on particle size and composition, some of them become activated; i.e. they continue growing even though the saturation ratio does not increase: a cloud droplet population has formed.

3.1. *Condensation model*

In the model the simultaneous condensation of water and nitric acid vapours occurs on the particles, which are chosen to be partly some insoluble substance and partly hygroscopic salt (e.g., ammonium nitrate) (see Fig. 1). The condensation model used in this study is based on the model used by Kulmala et al. (1993).

The rate of change of the droplet's total mass in the size class p (dm_p/dt) is obtained from the

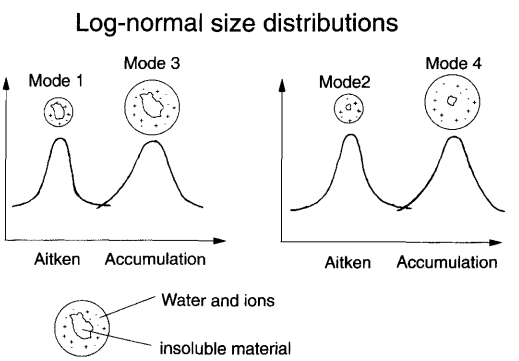

Fig. 1. Schematic picture of used four modes and multicomponent condensation on a mixed particle.

equation

$$\frac{dm_p}{dt} = I_{1,p} + I_{2,p}, \quad (1)$$

and the rate of change of the nitric acid mass fraction ($X_{2,p}$) in the liquid from

$$\frac{dX_{2,p}}{dt} = \frac{-X_{2,p} I_{1,p} + (1 - X_{2,p}) I_{2,p}}{(m_p - m_{p,\mathrm{ins}})}, \quad (2)$$

where $m_{p,\mathrm{ins}}$ is the mass of insoluble substance in the droplet. The mass fraction of salt in liquid mixture is calculated as a fraction of the initial mass of salt and total mass of solution (a sum of masses of water, salt and nitric acid). Then the mass fraction of water in the droplet is easily obtained with the aid of salt and nitric acid mass fractions.

The net mass fluxes $dm_{i,p}/dt \equiv I_{i,p}$, which are the rates at which masses of species i pass through a surface area of a droplet in the size class p can be calculated from following equations:

$$I_{1,p} = \frac{(1 - B_{22}) A_1 (S_1 - S_{a1}) + B_{12} A_2 (S_2 - S_{a2})}{1 - B_{22} - B_{11} + B_{11} B_{22} - B_{12} B_{21}},$$

$$I_{2,p} = \frac{(1 - B_{11}) A_2 (S_2 - S_{a2}) + B_{21} A_1 (S_1 - S_{a1})}{1 - B_{22} - B_{11} + B_{11} B_{22} + B_{12} B_{21}}, \quad (3)$$

where

$$A_i = \frac{-4\pi a_p M_{vi} \beta_{Mi} D_i p_{vei}(T_\infty)}{R T_\infty},$$

$$B_{ij} = \frac{S_{ai} L_i L_j M_{vi}}{4\pi a_p \beta_T K R T_\infty^2} A_i. \quad (4)$$

In the preceeding expressions $M_{v,i}$ is the molecular mass of species i, L_i is latent heat of vaporization, a_p is the droplet radius in the size class p, D_i is the vapour diffusion coefficent of species i in the carrier gas, S_i is the gas phase activity, S_a is the activity over the droplet surface (i.e., liquid phase activity × Kelvin effect), $p_{ve}(T_\infty)$ is the saturation vapour pressure at T_∞ and K is thermal conductivity of gas mixture. β_M and β_T are the transitional correction factors for mass and heat transfer respectively. We have adopted these factors from Fuchs and Sutugin (1970).

The preceeding expressions couples heat and mass transfer of water and nitric acid. The heat transfer is mainly due to release of latent heat of water vapour, since the condensation rate of water is much higher than the condensation rate of nitric acid.

3.2. *Numerical model and the physico-chemical data*

The set of ordinary differential equations is solved numerically using NAG-library FORTRAN-routine D02EAF (NAG, 1989). It uses a variable order, variable step method implementing the backward differentiation formulae (Hall and Watt, 1976). We have used 39 size classes in our simulations per log-normal distribution. The so-called moving boundary system has been used in simulations of the evolving size distributions (Kulmala et al., 1993).

The computer model for condensational growth of monodisperse aerosol particles, which is the basis of the condensational part of our cloud model described above has been tested previously by comparing the particle growth rates with experiments carried out at the University of Vienna (Rudolf et al., 1991; Rudolf, 1994). The experiments have been performed using expansion cloud chamber and CAMS-technique (Constant Angle Mie Scattering) (Wagner, 1985). The agreement between model results and experiments for growth rates in various binary systems (water — alcohol, water — nitric acid) was found to be within 0.5% (Rudolf et al., 1991; Rudolf, 1994, Vesala and Kulmala, 1993).

In the present simulation we have used ammonium nitrate as the hygroscopic material. Ammonium sulfate ($(NH_4)_2SO_4$) would have been the most relevant hygroscopic salt for this study, but there is no reliable physico-chemical data available for H_2O-$(NH_4)_2SO_4$-HNO_3 liquid mixtures, and without accurate thermodynamic data we would have artifacts in our numerical results. However, there exist reliable correlations for activity coefficients of H_2O-NH_4^+-H^+-NO_3^- solutions (S. Clegg, personal communication). So, as the soluble salt we have used NH_4NO_3, which is one of the substances commonly found in atmospheric aerosol particles (Götz et al., 1991). Moreover, its hygroscopic properties are very similar to those of ammonium sulphate (Low, 1969).

In previous studies, we have also simulated the system consisting NaCl as a salt and HCl and water condensing on it (Kulmala et al., 1994). The general results using that system and the system used in this study agree well with each other.

We need activity coefficents to be able to calculate activities, which are needed for S_{ai} in eq. (3).

The equilibrium solubility of HNO_3 in the droplets, for given partial pressure $p(HNO_3)$ (atm) is given by:

$$HNO_3 = H^+(aq) + NO_3^-(aq), \quad (5)$$

with a overall solubility constant (K_{H_x}/atm) defined by:

$$K_{H_x} = \frac{f_H f_{NO_3^-} X_{H^+} X_{NO_3^-}}{p(HNO_3)}, \quad (6)$$

where f_H is the activity coefficent for hydrogen ions in liquid, f_{NO3^-} is the activity coefficent for nitrate ions in the aqueous phase and X_{H^+} is the mole fraction of hydrogen ions in the aqueous phase and $X_{NO_3^-}$ mole fraction of nitrate ions in aqueous phase respectively. K_{H_x} is a function of temperature and its value is equal to 853.1 atm^{-1} at 298 K (Clegg and Brimblecombe, 1990). Activity coefficents of H^+ and NO_3^- in the aquous H-NH_4-NO_3 were calculated using the model of Pitzer, Simonson and Clegg (Clegg and Pitzer, 1992), with parameters for H-NO_3 and NH_4^- interactions based upon fits of the model equations to literature data for both solutes (Clegg and Pitzer, 1992).

The other physico-chemical data needed for calculations were adopted from the literature (ICT, 1927; Landoldt-Börnstein, 1960; Timmermans, 1960; Duisman and Stern, 1969; Kell, 1975; CRC, 1985; Kaye and Laby, 1986 and Reid et al., 1987) and are presented in Appendix A.

4. Radiative properties of cloud droplet distribution

Particle phase and gas phase hygroscopicity influence the number of cloud droplets (Korhonen et al., 1994). This affects the optical thickness (τ) of the cloud. Assuming the scattering efficiency of cloud droplets is 2 for visible wavelengths (Hansen and Travis, 1974) we can approximate the relationship between optical thickness τ and the number concentration of cloud droplets (N) using following expression

$$\tau = H\left(\frac{9\pi(LWC)^2 N}{2\rho^2}\right)^{1/3}, \quad (7)$$

where ρ is the density of liquid water, LWC is the liquid water content and H is the cloud depth.

The albedo of the cloud (A), i.e., the ratio of the backward reflected radiation to the incoming radiation, can be estimated from the equation presented by Lacis and Hanssen (1974)

$$A = \frac{\tau}{7.7+\tau}. \quad (8)$$

Eqs. (7) and (8) are rough approximations. However, we have made calculations with more detailed radiative transfer models based on the Slingo's (1989) optical constant's parameterization, delta-Eddington code and two-stream approximation presented by Lacis and Hanssen (1974). If we compare results from more detailed model to the results given by eq. (7) and eq. (8), we notice that results from simple eqs. ((7) and (8)) are qualitatively reasonable.

The sensitivity of optical thickness and albedo to N at constant liquid water content and cloud height is given by

$$\frac{\Delta\tau}{\tau} = \frac{\Delta N}{3N}, \quad (9)$$

$$\frac{dA}{dN} = \frac{A(1-A)}{3N}. \quad (10)$$

Thus, for given N the most susceptible clouds are those with A around 0.5. However the maximum of dA/dN is rather flat: for $A=0.25$ or $A=0.75$, dA/dN is still 3/4 of its maximum value (Twomey, 1991).

In the present paper, we discuss variations in cloud reflectance due to changes of cloud droplet concentration. In this case no new cloud is involved and we can concentrate on the solar (visible) radiation wavelenghts. It is important to distinguish these effects (i.e. changes in the reflectance of existing clouds) from changes in cloud cover, since increasing cloudiness effects also on terrestial (infrared) radiation fluxes. Generally, when the LWC and the depth of cloud layer is kept constant, the increase in the amount of cloud droplets increases also the reflectance of the cloud. Furthermore if the number of droplets increases there can be an additional enhancement of the shortwave cooling, since it might also increse cloud lifetime (Albrecht, 1989; Twomey, 1991; Charlson and Wigley, 1994; Pincus and Baker, 1994).

5. Simulated cloud droplet concentrations and their effect on radiative properties of clouds

The formation and growth of a cloud droplet population due to binary condensation of water and nitric acid on partially soluble non-volatile particles were simulated. Totally more than 200 simulation runs have been performed. In the simulations the inital saturation ratio for water vapour was 0.99. The initial nitric acid concentration was between 0 and 10 ppbv. The initial air temperature varied from $-10°C$ to 20°C and pressure from 600 to 1000 mbar. The vertical updraft velocity varied from 0.1 to 1.0 m/s. We used artificial (but realistic) and measured lognormal number distributions (as a function of radius) of particles (a mixture of ammonium nitrate and some insoluble material). The geometric mean (dry) radius in Aitken mode varied from 10 to 40 nm and in accumulation mode from 50 to 135 nm. The geometric standard deviation varied from 1.3 to 2.5. The total number of aerosol particles varied from 75 to 12000 cm^{-3}. The fraction belonging to Aitken mode varied from 40 to 95%. In the Aitken mode we had between 20 and 80% of the particles in the less hygroscopic mode and from 5 to 50% in the accumulation mode.

A collection of different simulation results are presented in Figs. 2–6. The formation of cloud droplets is seen to be more efficient when the particle-phase or gas-phase hygroscopicity is increased. The clear effect of the soluble mass fraction can be seen, e.g., by comparing Figs. 2a and 2b (or 3a and 3b) with each other. This corroborates the results obtained by Korhonen et al., (1994).

Figs. 2 and 3 show the activated fraction of aerosol particles as a function of the total number of aerosol particles. The increase in activated number fraction with increasing updraft velocity can be seen by comparison of Figs. 2 and 3. The increase activated fraction with increasing nitric acid concentration can be seen from Figs. 2 and 3. We can see that the activated number fraction steeply decreased when aerosol concentration increases from 75 to 1500. After that the changes are smaller. However by increasing the total aerosol concentration we still increase the total number of cloud droplets. This effect is pronounced when we have realistic (varying) soluble mass fractions.

In each case, we are able to see the effect of nitric acid on the cloud droplet concentration. The effect is very clear even in polluted areas where we have high aerosol concentrations and high nitric acid concentrations. In cleaner areas where aerosol concentrations are smaller we are able to see the effect even if the nitric acid concentration is 0.1 ppbv.

As seen (Fig. 4.) the 4th mode (more hygroscopic, accumulation) dominates the formation process of cloud droplets. This is especially true when the number concentration of aerosol particles is high. There are some conditions, when also modes 2 and 3 play some rŏle (see Fig. 4.)

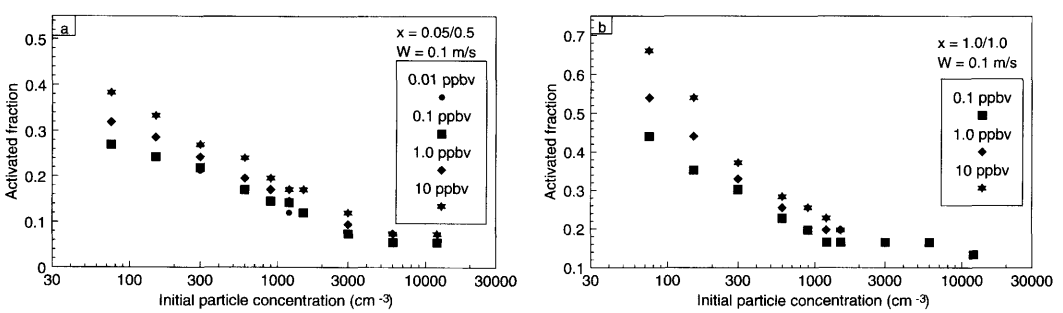

Fig. 2. Activated fraction as a function of initial aerosol particle concentration. In (A), the initial soluble salt mass fraction ($X_{m,i}$) in the less hygroscopic modes (1 and 3) is 0.05 and more hygroscopic modes (2 and 4) is 0.5. Modes 1 and 2 belong to Aitken mode and modes 3 and 4 to accumulation mode. 2/3 of particles belong to the Aitken mode. In the Aitken mode, 60% of the particles belong to the less hygroscopic mode compared with 30% in accumulation mode. In (B), the initial soluble mass fraction is 1.0 in all modes. The initial amount of gaseous HNO_3 and aerosol particles in the parcel have been varied. The dry mean radius was 30 nm in the Aitken mode and 100 nm in the accumulation mode. The standard deviation was 1.35 in Aitken and 1.6 in accumulation mode. The updraft velocity was 0.1 m/s and temperature 20°C.

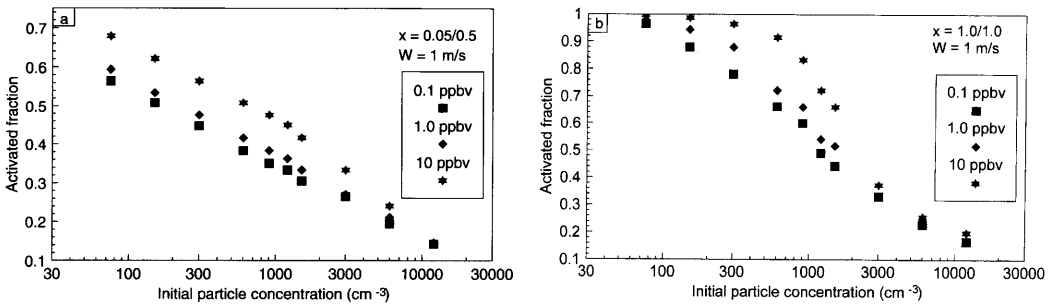

Fig. 3. Activated fraction as a function of initial aerosol particle concentration. In (A), the initial soluble salt mass fraction ($X_{m,i}$) in the less hygroscopic modes (1 and 3) is 0.05 and more hygroscopic modes (2 and 4) is 0.5. Modes 1 and 2 belong to Aitken mode and modes 3 and 4 to accumulation mode. 2/3 of particles belong to the Aitken mode. In the Aitken mode 60% of the particles belong to the less hygroscopic mode compared with 30% in accumulation mode. In (B), the initial soluble mass fraction is 1.0 in all modes. The initial amount of gaseous HNO_3 and aerosol particles in the parcel have been varied. The dry mean radius was 30 nm in the Aitken mode and 100 nm in the accumulation mode. The standard deviation was 1.35 in Aitken and 1.6 in accumulation mode. The updraft velocity was 1.0 m/s and temperature 20 °C.

This is typical for high acid concentration, low aerosol particle concentration and higher updraft velocity.

The competition between modes 2 and 3 is clear. Some hygroscopic particles from the Aitken mode have larger probabilities to activate than do the less hygroscopic particles in the accumulation mode. If we ignore the Kelvin effect the relation is clear: the particle having the larger soluble mass will activate first so

$$X_{2,1}a_1^3 \geqslant X_{2,2}a_2^3 . \qquad (11)$$

The Kelvin effect will change this behaviour somewhat to make it easier for accumulation mode particles to win the competition. Practically no particles will activate from mode 1.

In Fig. 4a, we are able to see how mode 2 (more hygroscopic, Aitken) has a significant role at initial nitric acid concentration 10 ppbv. It is even more important than mode 4 if the initial aerosol concentration is less than 300 cm^{-3} and more important than mode 3 until particle concentration is more than several thousand. In Figs. 4b and c, when the nitric acid concentration is 1 ppbv and 0.1 ppbv respectively, mode 2 does not have such a significant rõle.

From Table 1, we are able to see how the initial fraction between each mode will affect number of cloud droplets. As above the most important is mode 4 (the more hygroscopic, accumulation). The number concentration in this mode determines how great a fraction in modes 2 and 3 can be activated. This is seen by comparing case A and B in Table 1.

In Figs. 5 and 6, activated fractions in each mode as a function of total initial aerosol concentration are shown. With an updraft velocity of 0.1 m/s almost all cloud droplets come from mode 4 and the activated fraction of mode 4 is near unity with low particle concentration. With updraft velocity 1.0 m/s (Fig. 6) also the activated fraction of modes 2 and 3 are near one with low particle concentration. This shows clearly that in some atmospheric conditions other modes than mode 4 influence on cloud droplet concentrations.

We have also compared our results to experimental data. Gillani et al., (1992a, 1992b) have determined the activated fraction in continental stratiform clouds. They have observed the activated fraction of accumulation mode particles varies from 0.1 to 1.0 and is a function of particle concentration. These observations agree nicely with our simulations. Noone et al. (1992) have observed that in fog conditions in Po Valley ca 1 to 8% of particles will activate when the total number concentration in accumulation mode was around 6000 cm^{-3}. According to our simulations the activated fraction in this polluted situation was near 5%. In the cleaner air the activated fraction is typically much bigger according to our simulations and according to experiments (Heintzenberg et al., 1989 and Hallberg et al., 1994).

In Table 2, the simulated fraction of cloud drop-

Table 1. *The total number of activated cloud droplets and the fraction of cloud droplets in modes 1,2,3 and 4, when the initial soluble salt mass fraction ($X_{m,i}$) is varying*

Updraft vel. (m/s)	HNO_3 (ppb)	$X_{m,lh}$	$X_{m,mh}$	Fraction of droplets mode 1	Fraction of droplets mode 2	Fraction of droplets mode 3	Fraction of droplets mode 4	Actual total (cm^{-3})
(A)								
1.0	10.00	0.05	0.50	0.0651	0.6576	0.1897	0.0876	342.14
1.0	1.00	0.05	0.50	0.0159	0.6169	0.2428	0.1244	240.24
1.0	0.10	0.05	0.50	0.0094	0.5864	0.2598	0.1444	206.17
1.0	0.01	0.05	0.50	0.0094	0.5864	0.2598	0.1444	206.17
0.1	10.00	0.05	0.50	0.0003	0.3658	0.3477	0.2862	100.09
0.1	1.00	0.05	0.50	0.0005	0.2184	0.3924	0.3886	71.56
0.1	0.10	0.05	0.50	0.0000	0.1032	0.4034	0.4935	53.92
0.1	0.01	0.05	0.50	0.0000	0.0675	0.3520	0.5806	45.83
0.1	0.00	0.05	0.50	0.0000	0.0675	0.3520	0.5806	45.83
1.0	10.00	0.50	0.50	0.6096	0.2612	0.0904	0.0388	771.33
1.0	1.00	0.50	0.50	0.5618	0.2407	0.1388	0.0593	502.34
1.0	0.10	0.50	0.50	0.5341	0.2289	0.1659	0.0711	415.86
1.0	10.00	0.05	0.05	0.3224	0.1382	0.3777	0.1618	177.04
1.0	1.00	0.05	0.05	0.1210	0.0519	0.5789	0.2482	107.23
1.0	0.10	0.05	0.05	0.0729	0.0313	0.6271	0.2688	99.00
1.0	0.01	0.05	0.05	0.0771	0.0330	0.6229	0.2669	93.62
(B)								
1.0	10.00	0.05	0.50	0.0459	0.7219	0.0640	0.1682	415.58
1.0	1.00	0.05	0.50	0.0056	0.6727	0.0851	0.2374	293.72
1.0	0.10	0.05	0.50	0.0031	0.6337	0.0902	0.2729	254.53
0.1	10.00	0.05	0.50	0.0000	0.2132	0.1231	0.6638	97.76
0.1	1.00	0.05	0.50	0.0000	0.0941	0.1182	0.7876	78.82
0.1	0.10	0.05	0.50	0.0000	0.0325	0.1025	0.8650	67.42
0.1	0.01	0.05	0.50	0.0000	0.0335	0.0749	0.8916	65.41
(C)								
1.0	10.00	0.05	0.50	0.0182	0.4386	0.2172	0.3260	367.50
1.0	1.00	0.05	0.50	0.0168	0.3393	0.2415	0.4176	285.21
1.0	0.10	0.05	0.50	0.0086	0.2972	0.2403	0.4616	256.27
0.1	10.00	0.05	0.50	0.0000	0.0321	0.2014	0.7665	138.81
0.1	1.00	0.05	0.50	0.0000	0.0108	0.1700	0.8193	122.03
0.1	0.10	0.05	0.50	0.0000	0.0031	0.0973	0.8995	102.09
0.1	0.01	0.05	0.50	0.0000	0.0035	0.1076	0.8889	92.38

Modes 1 and 2 belong to the Aitken mode and modes 3 and 4 to the accumulation mode. The initial amount of gaseous HNO_3 has been varied. The initial mean radius was 30 nm in Aitken mode and 100 nm in accumulation mode. The standard deviation was 1.35 in Aitken and 1.6 in accumulation mode. The temperature was 20°C. (A) refers to number concentration of 1000 in Aitken mode and 100 in accumulation mode. 70% of particles were less hygroscopic. (B) refers to number concentration of 1000 in Aitken mode (600 less hygroscopic and 400 more hygroscopic) and 100 in accumulation mode (30+70). (C) refers to number concentration of 600 in Aitken mode (360+240) and 210 in accumulation mode (90+120).

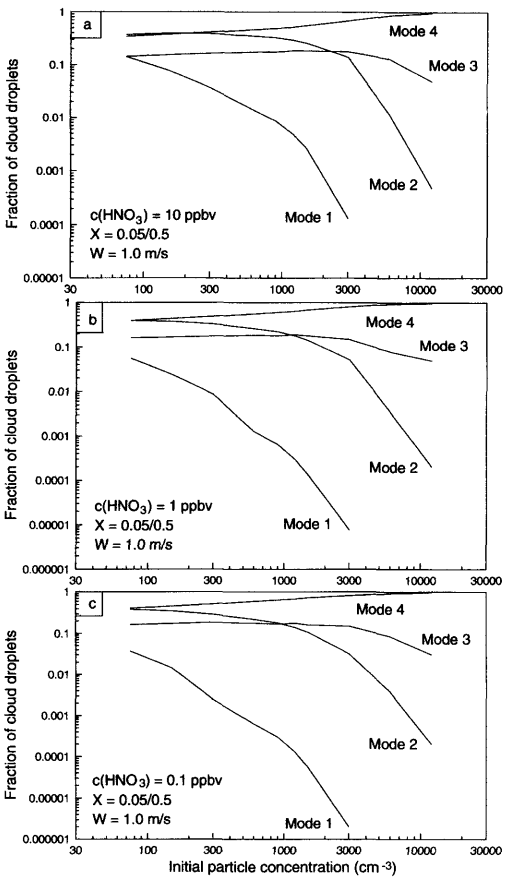

Fig. 4. Fraction of cloud droplets in each mode as a function of initial aerosol particle concentration. Updraft velocity is 1.0 m/s and the mass fraction of soluble material is 0.05 in the less hygroscopic modes (1 and 3) and 0.5 in the more hygroscopic modes (2 and 4). Other parameters are given in Fig. 3. Initial nitric acid concentrations are 10 ppbv (a), 1 ppbv (b) and 0.1 ppbv (c).

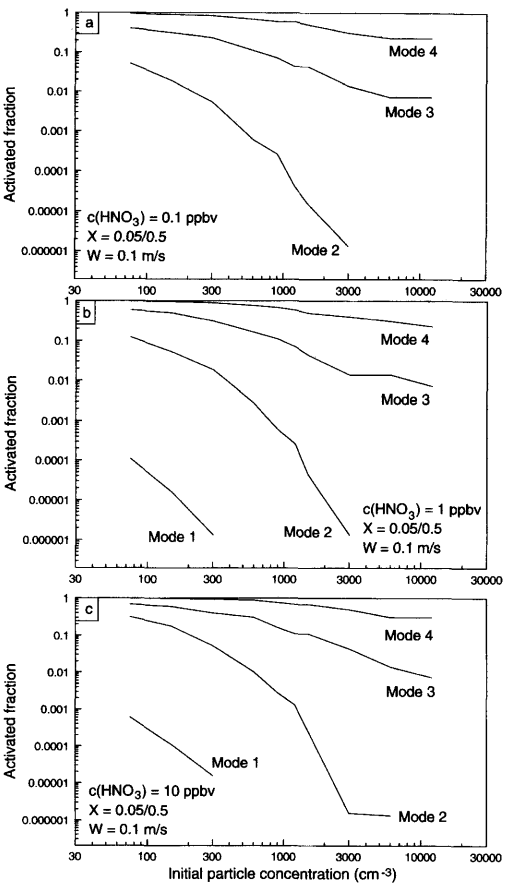

Fig. 5. Activated fraction in each mode as a function of initial aerosol particle concentration. Parameters used in simulations are given in Fig. 2. Initial nitric acid concentrations are 0.1 ppbv (a), 1 ppbv (b) and 10.0 ppbv (c).

lets and number of cloud droplets are presented using two measured distributions as initial size distributions of aerosol particles. The initial size distributions were measured in Kleiner Feldberg, Germany, during a field campaign (Svenningsson et al., 1994). In previous studies the soluble mass fraction has been determined using impactors (see Seidl, 1994). Thus we also have simulated (see Table 2) the situation when the soluble mass fraction will change from accumulation mode to Aitken mode, but is the same within the modes. In this case the accumulation mode dominates the activation process. The situation is different if we use bimodality in size and in hygroscopicity as we can see from Table 2.

The change in the optical thickness can be obtained from Equation 9. The change of optical thickness under conditions of high nitric acid concentration (10 ppbv) and due to the change in soluble mass fraction of particulate matter is seen in Figs. 7 and 8. The basic level to which the change of optical thickness has been calculated is that the soluble mass fraction is 1 and nitric acid concentration 0 ppbv. If we used more realistic (i.e., observed) values for soluble mass fraction the optical thickness will decrease. In some cases the increase of nitric acid concentration from 0 ppbv to 10 ppbv is able to cancel this effect. This is the

Table 2. *The total number of activated cloud droplets and the fraction of cloud droplets in modes 1,2,3 and 4, when the initial soluble salt mass fraction ($X_{m,i}$) is varying*

Updraft vel. (m/s)	HNO_3 (ppb)	$X_{m,lh}$	$X_{m,mh}$	Fraction of droplets mode 1	Fraction of droplets mode 2	Fraction of droplets mode 3	Fraction of droplets mode 4	Actual total (cm^{-3})
Nov. 1								
(1)				0.6080	0.2710	0.0347	0.0863	1686.40
1.0	10.00	0.05	0.50	0.0781	0.4502	0.1266	0.3451	421.63
1.0	1.00	0.05	0.50	0.0501	0.4144	0.1131	0.4204	345.60
1.0	0.10	0.05	0.50	0.0510	0.4218	0.1001	0.4271	339.48
1.0	0.01	0.05	0.50	0.0257	0.4330	0.1028	0.4385	330.68
1.0	10.00	1.00	1.00	0.3411	0.3556	0.0870	0.2163	672.60
1.0	1.00	1.00	1.00	0.2822	0.3460	0.1066	0.2652	548.59
1.0	0.10	1.00	1.00	0.3084	0.2853	0.1165	0.2897	501.88
1.0	0.01	1.00	1.00	0.3085	0.2853	0.1165	0.2897	501.86
Nov. 12								
(2)				0.3730	0.3918	0.0568	0.1784	2074.50
0.1	10.00	0.05	0.50	0.0000	0.0617	0.0007	0.9376	278.48
0.1	1.00	0.05	0.50	0.0000	0.0388	0.0004	0.9608	238.14
0.1	0.10	0.05	0.50	0.0000	0.0237	0.0002	0.9761	198.85
1.0	10.00	0.05	0.50	0.0144	0.4711	0.0653	0.4492	822.59
1.0	1.00	0.05	0.50	0.0050	0.3742	0.0386	0.5822	631.24
1.0	0.10	0.05	0.50	0.0027	0.3051	0.0431	0.6492	566.08
1.0	0.01	0.05	0.50	0.0027	0.3103	0.0311	0.6560	556.53
0.1	10.00	1.00	1.00	0.0092	0.0501	0.0964	0.8443	342.88
0.1	1.00	1.00	1.00	0.0092	0.0501	0.0964	0.8443	342.88
0.1	0.10	1.00	1.00	0.0100	0.0546	0.1051	0.8303	314.48
1.0	10.00	1.00	1.00	0.2212	0.3460	0.1029	0.3299	1120.00
1.0	1.00	1.00	1.00	0.1558	0.2786	0.1305	0.4351	847.70
1.0	0.10	1.00	1.00	0.3687	0.2791	0.1307	0.4342	846.40
(3) 0.1	10.00	0.33	0.47	0.0025	0.0176	0.1236	0.9771	267.23
(3) 0.1	1.00	0.33	0.47	0.0012	0.0091	0.0693	0.9204	248.59
(3) 0.1	0.10	0.33	0.47	0.0006	0.0109	0.0559	0.9326	208.13
(3) 1.0	10.00	0.33	0.47	0.1548	0.2769	0.1352	0.4331	853.10
(3) 1.0	1.00	0.33	0.47	0.0830	0.2449	0.1510	0.5211	705.20
(3) 1.0	0.10	0.33	0.47	0.0907	0.1867	0.1566	0.5660	645.00

Modes 1 and 2 belong to Aitken mode and modes 3 and 4 to accumulation mode. The input distributions were measured at Kleiner Feldberg (Svenningsson et al., 1994) (1) Refers to the measured number concentrations. Nov. 1: mode 1: the initial mean radius was 12.8 nm and the standard deviation was 2.31: Mode 2: the initial mean radius was 23.5 nm and the standard deviation was 2.309: Mode 3: the initial mean radius was 90.3 nm and the standard deviation was 1.361: Mode 4: the initial mean radius was 95.2 nm and the standard deviation was 1.393 (2) Nov. 12: Mode 1: the initial mean radius was 29.0 nm and the standard deviation was 1.571. Mode 2: the initial mean radius was 33.8 nm and the standard deviation was 1.664. Mode 3: the initial mean radius was 77.3 nm and the standard deviation was 1.447. Mode 4: the initial mean radius was 127.9 nm and the standard deviation was 1.518. (3) Refers to uniform soluble mass fraction in Aitken mode and in accumulation mode.

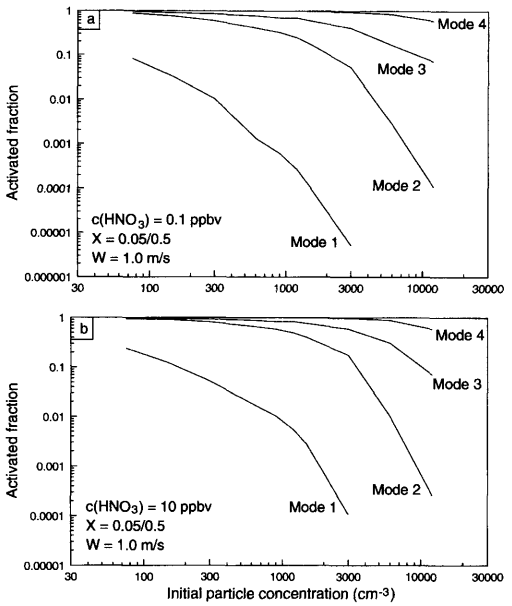

Fig. 6. Activated fraction in each mode as a function of initial aerosol particle concentration. Parameters used in simulations are given in Fig. 3. Initial nitric acid concentrations are 0.1 ppbv (a) and 10.0 ppbv (b).

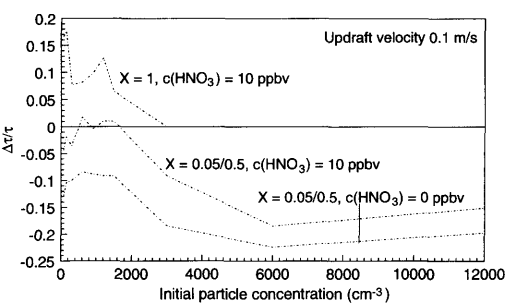

Fig. 7. $\Delta\tau/\tau$ as a function of initial aerosol particle concentration. The basic level to which the change of optical thickness has been calculated is that the soluble mass fraction is 1 and nitric acid concentration 0 ppbv. Parameters used in simulations are given in Fig. 2.

case when aerosol concentration is near 1000 with updraft velocity 0.1 m/s (Fig. 7) and when concentration is between 2000 and 6000 with updraft velocity 1.0 m/s (Fig. 8). When the aerosol concentration is smaller the nitric acid is not able to activate so many new particles that optical thickness will increase as much as it will decrease due

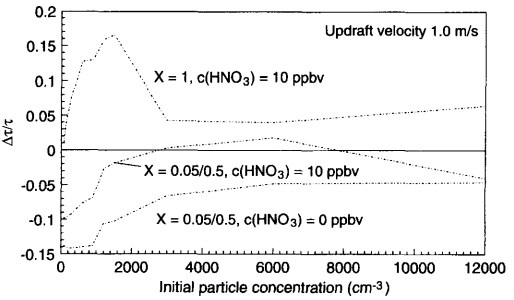

Fig. 8. $\Delta\tau/\tau$ as a function of initial aerosol particle concentration. The basic level to which the change of optical thickness has been calculated is that the soluble mass fraction is 1 and nitric acid concentration 0 ppbv. Parameters used in simulations are given in Fig. 3.

to the decrease of soluble mass fraction. In moderate aerosol concentrations the nitric acid effect is most significant. With smaller updraft velocity the available water supersaturation is smaller and thus the compensation appears at smaller aerosol concentration. The microscopic structure (small peaks) in the plots are due to numerical inaccurancy, since we have only 4×39 size classes in our simulations. Thus activation does not occur smoothly.

6. Conclusions

The effect of particle phase and gas phase hygroscopicity on the formation and properties of cloud droplets is clearly seen in the present simulations. Generally, this study shows that the increase in hygroscopicity implies an increasing number of cloud droplets and increasing optical thickness of a cloud. How the soluble mass is distributed in aerosol particles and between modes also seems to be important (Ogren and Charlson, 1992).

The number concentration and distribution characteristics of four aerosol modes are taken from experiments and from the literature. The importance of particle phase hygroscopicity and clear evidence of the importance of gas phase hygroscopicity enables us to suggest that the hygroscopicity should be included in the different types of models to clarify the regional and global (direct and indirect) effects of aerosols on radiation balance.

The common use of uniform soluble mass fraction of aerosols is shown to be misleading. If the soluble mass fraction of 1 or 0.5 is used the number concentration of cloud droplets and the optical thickness of clouds are overestimated compared with measured soluble fractions. The hygroscopic bimodality also changes the common picture of activation. If we have uniform hygroscopicity only particles belonging to accumulation mode are able to form cloud droplets. In the case of bimodal hygroscopicity also a significant fraction of Aitken mode particles will form cloud droplets particularly at low aerosol loadings.

The estimation of global indirect forcing due to the effect of soluble mass fraction or condensable gases on cloud droplet formation is important to do in future. The task is more difficult than the estimation of the indirect sulfate effect (Boucher and Lohmann, 1995), since to determine the change of hygroscopic properties of aerosol particles over centuries we need to know the emissions of soluble and insoluble material into atmosphere.

7. Acknowledgements

Support of this work by the Academy of Finland and the help of Dr. S. Clegg, Mr. P. Aalto are gratefully acknowledged.

8. Appendix A

Physico-chemical data

The physico-chemical data needed for calculations were adopted from the literature (ICT, 1927; Landoldt-Börnstein, 1960; Timmermans, 1960; Duisman and Stern, 1969; Kell, 1975; CRC, 1985; Kaye and Laby, 1986 and Reid et al., 1987).

Liquid density: (kg/m^3, t in °C):

$$\rho_{H_2O}=(999.83952+16.945176t - 7.9870401\cdot 10^{-3}t^2 - 46.170461\cdot 10^{-6}t^3+105.56302\cdot 10^{-9}t^4 - 280.54253\cdot 10^{-12}t^5)/(1+16.879850.10^{-3}t).$$

Surface Tension N/m, and T in K):

$$\sigma_{H_2O}=0.117296-T\cdot 0.152362\times 10^{-3}.$$

Saturation vapour pressures (Nm^{-2}, T in K) for water and nitric acid:

$$p_{H_2O}=\exp\{77.34491296-7235.424651/T - 8.2\ln T+T\cdot 5.7113\times 10^{-3}\}$$

$$p_{HNO_3}=\exp\left\{22.430-\frac{3422.190}{T-43.0}\right\}.$$

Vaporization enthalpies (or specific latent heat of vaporization) L in J/kg and T in K:

$$L_{H_2O}=3.14566\times 10^6-T\cdot 2.36164\times 10^3,$$

$$L_{HNO_3}=4.5150\times 10^5.$$

Binary Diffusion Coefficient is calculated with following equation

$$D(p_0,T)=D_N\left(\frac{T}{T_n}\right)^{\mu}\frac{p_N}{p_0}.$$

Here $T_N=273.15$ K, $p_N=101324.72$ Pa. D_n is 22.07487×10^{-6} m^2/s for water in air and 12.98×10^{-6} m^2/s for nitric acid in air. The values for μ are 1.6658 and 1.75, correspondingly.

The thermal conductivity ($Wm^{-1}K^{-1}$, T in K):

$$K_{air}=3.4405\times 10^{-3}+T\cdot 7.5177\times 10^{-5},$$

$$K_{H_2O}=-6.7194\times 10^{-3}+T\cdot 7.4857\times 10^{-5}.$$

The thermal conductivity of gas mixture is estimated using methods given in Reid et al. (1987).

9. Appendix B

Nomenclature

The following symbols are used in the text most frequently.

Symbol	Meaning
a_p	droplet radius
A	albedo of the cloud
A_i	factors determined in eq. (4) and used in eq. (3).
B_{ij}	factors determined in eq. (4) and used in eq. (3).
D_{ij}	binary diffusion coefficient at temperature T_∞
f_i	activity coefficient
H	the cloud depth
$I_{i,p}$	mass flux directed to the droplet (size class p)

K	thermal conductivity	$X_{2,p}$	mass fraction of nitric acid in a droplet (size class p)
L_i	latent heat of vaporization	β_{Mi}	transitional correction factor for mass transfer
LWC	the liquid water content	β_T	transitional correction factor for heat transfer
m_p	mass of a droplet	τ	the optical thickness
M_i	molecular weight	ρ	density of liquid water
N	the number concentration of cloud droplets	subscripts	
$p_{v,i}$	partial vapour pressure	i	species
p_{vei}	saturation vapour pressure over a flat surface	ins	insoluble
R	gas constant, 8.314 J/mole K	j	species
S_i	gas phase activity	l	liquid
S_{ai}	activity over the droplet surface	p	size class
t	time	v	vapour
T	temperature	∞	value far from the droplet
X_i	mole fraction		

REFERENCES

Albrecht, B. A. 1989. Aerosols, cloud microphysics, and fractional cloudiness. *Science* **245**, 1277–1230.

Boucher, O. and Lohmann, U. 1995. The Sulfate-CCN-CLOUD albedo effect: a sensitivity study with two general circulation models. *Tellus* **47B**, 281–300.

Charlson, R. J. and Wigley, T. M. L. 1994. Sulfate aerosol and climatic change. *Scientific American* **2**, 48–57.

Charlson, R. J., Lagner, J. Rodhe, H., Leovy, C. B. and Warren S. G. 1991. Perturbation of northern hemisphere radiative balance by backscattering from anthropogenic sulfate aerosols. *Tellus* **43AB**, 152–163.

Charlson, R. J., Schwartz, S. E., Hales, J. M., Cess, R. D., Coakley, Jr., J. A., Hansen, J. E. and Hofmann, D. J. 1992. Climate forcing by antropogenic aerosols. *Science* **255**, 423–430.

Clegg, S. L. and Brimblecombe, P. 1990. Equilibrium Partial pressures and Mean Activity and Osmotic Coefficents of 0–100% Nitric Acid as a function of Temperature. *J. Phys. Chem.* **94**, 5369–5380.

Clegg, S. L. and Pitzer, K. S. 1992. Thermodynamics of multicomponent, miscible, ionic solutions: Generalized equations for symmetrical electrolytes. *J. Phys. Chem.* **96**, 3513–3520.

CRC *Handbook of Chemistry and physics*, 1985, 66th edition. The Chemical Rubber Co, Cleveland, Ohio.

Curry, J. A. 1995. Interactions among aerosols, clouds and climate of the Artic Ocean. *The Science of the Total Environment*, in press.

Duisman, J. A. and Stern, S. A. 1969. Vapor pressure and boiling point of pure nitric acid. *J. Chem. Eng. Data* **14**, 457.

FORTRAN-routine D02EAF, 1989. The NAG Fortran Library Manual Mark 14, 2. The Numerical Algorithms Group Ltd., Oxford.

Fuchs, N. A. and Sutugin, A. G. 1970. *Highly dispersed aerosols.* Ann Abor Science Publ., Ann Abor, Michigan, 105 p.

Gillani, N. V., Daum, P. H., Schwartz, S. E., Leaitch, W. R., Strapp, J. W. and Isaac, G. A. 1992a. Fractional activation of accumulation-mode particles in warm continental stratiform clouds. *Precipitation scavenging and atmosphere surface exchange*, ed. S. E. Schwartz and W. G. N. Slinn. Hemisphere, Washington DC, Vol 1., 345–358.

Gillani, N. V., Schwartz, S. E., Daum, P. H., Leaitch, W. R., Strapp, J. W. and Isaac, G. A. 1992b. *Fractional activation of accumulation-mode aerosols in Continental stratiform clouds.* Presented at the WMO Workshop on Cloud Microphysics and Global Change.

Götz, G., Mèszáros, E. and Vali, G. 1991. *Atmospheric particles and nuclei.* Akadiai Kiadó, Budapest.

Hall, G. and Watt, J. M. (eds.) 1976 *Modern numerical methods for ordinary differential equations*, pp. 154–158 Clarendon, Oxford.

Hallberg, A., Noone, K. J., Ogren, J. A., Svenningsson, I. B., Flossmann, A., Wiedensohler, A., Hansson, H.-C., Heintzenberg, J., Anderson, T. L., Arends, B. G. and Maser, R. 1994. Phase partioning of aerosol particles in cloud at Kleiner Feldberg. *J. Atmos. Chem.* **19**, 107–127.

Hansen, J. E. and Travis, L. D. 1974. Light scattering in planetary atmospheres. *Space Sci. Rev.* **16**, 527–610.

Hansson H.-C., Svenningsson B., Martinsson B., Swietlicki E. and Wiedensohler A. 1994. Icorporation of aerosols and clouds. *The Proceedings of EUROTRACK Symposium '94*, ed. P. M. Borrell et al., pp. 984–988.

Hartmann, D. L. and Doelling, D., 1991. On the net radiative effectiveness of clouds. *J. Geophys. Res.* **96**, 869–891.

Heintzenberg, J., Ogren, J. A., Noone, K. J. and Gärdneus, L. 1989. The size distribution of submicrometer particles withi and about stratocumulus cloud droplets

on Mt. Åreskutan, Sweden. *Atmospheric Research* **24**, 89–101.

ICT, *International Critical Tables, 1927* vol. 3. McGraw-Hill, New York.

Kaye, G. W. C. and Laby, T. H. 1986. *Tables of physical and chemical constants.* Longman Group Ltd., New York.

Kell, G. S. (1975) Density, thermal expansivity and compressibility of liquid water from 0° to 150°C: Correlations and tables for atmospheric pressure and saturation reviewed and expressed on 1968 temperature scale. *J. Chem. Eng. Data* **20**, 97–105.

Kim, Y. and Cess, R. D. 1993. Effect of anthropogenic sulfate aerosols on low-level cloud albedo over oceans. *J. Geophys. Res.* **98**, 14883–14887.

Korhonen, P., Kulmala, M., Hansson, H.-C., Svenningsson, I. B. and Rusko, N. 1995. Hygroscopicity of preexisting particle distribution and formation of cloud droplets: a model study. *Atmospheric Research*, in press.

Kulmala, M., Laaksonen, A., Korhonen, P., Vesala, T., Ahonen, T. and Barrett, J. C. 1993. The effect of atmospheric nitric acid vapor on cloud condensation nucleus activation. *J. Geophys. Res.* **98**, 22949–22958.

Kulmala, M., Korhonen, P., Laaksonen, A., Vesala, T., Aalto, P., Mäkelä, J., Hämeri, K. and Keronen, P. 1994. Chemical and physical conversion in cold atmosphere and the effect of radiation. In: *The Finnish Research Programme on Climate change,* 2nd progress report, Publication of the Academy of Finland 1/94, Painatuskeskus oy, Helsinki.

Kulmala, M., Korhonen, P., Laaksonen, A., Vesala, T. 1995. Changes in cloud properties due to NO_x emissions. *Geophys. Res. Lett.* **22**, 239–242.

Lacis, A. A. and Hansen, J. E. 1974. A parametrization for the absorption of solar radiation in the earth's atmosphere. *J. Atmos. Sci.* **31**, 118–133.

Landoldt-Börnstein, 1960. *Zahlenwerte und Functionen aus Physik-Chemie-Astronomie-Geophysik-Technik.* Springer-Verlag, Berlin.

Leaitch W. R., Isaac, G. A., Strapp, J. W., Banic, C. M. and Wiebe, H. A. 1992. The relationship between cloud droplet number concentrations and anthropogenic pollution: observations and climatic implications. *J. Geophys. Res.* **97**, 2463–2474.

Low, R. D. H. 1969. A theoretical study of nineteen condensation nuclei. *J. Rech. Atmos.* **4**, 65–67.

Noone, K. J., Ogren, J. A., Hallberg, A., Heintzenberg, J., Ström, J., Hansson, H.-C., Svenningsson, B., Wiedensohler, A., Fuzzi, S., Faccihini, M. C., Arends, B. G. and Berner, A. 1992. Changes in aerosol size- and phase distributions due to physical and chemical processes in fog. *Tellus* **44B**, 489–504.

Ogren, J. A. and Charlson, R. J. 1992. Implications for models and measurements of chemical inhomogeneities among cloud droplets. *Tellus* **44B**, 208–225.

Pincus, R. and Baker, M. B. 1994. Effect of precipitation on the albedo susceptibility of clouds in the marine boundary layer. *Nature* **372**, 250–252.

Pruppacher, H. R. and Klett, J. D. 1978. *Microphysics of clouds and precipitation.* D. Reidel Publishing Co., Holland.

Reid, R. C., Prausnitz, J. M., Poling, B. E. 1987. *The properties of gases and liquids,* 4th Edition. McGraw-Hill, New York.

Rudolf, R., Majerowicz, A., Kulmala, M., Vesala, T., Viisanen, Y. and Wagner, P. E., 1991. Kinetics of particle growth in supersaturated binary vapor mixtures. *J. Aerosol Sci.* **22**, S51–S54.

Rudolf, R. 1994. *Experimental investigation on condensation of supersaturated acid – Water vapor mixtures by means of laser light scattering in a newly developed expansion chamber.* Doctoral Dissertation, University of Vienna, Department of Experimental Physics.

Schwartz, S. E. 1988. Are global cloud albedo and climate controlled by marine phytoplankton? *Nature* **336**, 441–445.

Seidl, W. 1994. Initial cloud droplet number concentrations in clean and polluted areas: Simulation by a condensation model and comparison with measurements. *Atmospheric Research* **31**, 157–185.

Slingo, A. 1989. A GCM parametrization for the shortwave radiative properties of water clouds. *J. Atmos. Sci.* **46**, 1419–1427.

Stolzenburg, M. R. and McMurry, P. H. 1988. *TDMAFIT user's manual.* PTL Publications No 653, Particle Technology Laboratory, Department of Mechanical Eng., University of Minnesota, Minneapolis, MN, USA.

Svenningsson, I. B., Hansson, H.-C. Wiedensohler, A., Ogren, J. A., Noone, K. J. and Hallberg, A. 1992. Hygroscopic growth of aerosol particles in the Po-valley. *Tellus* **44B**, 556–569.

Svenningsson, I. B., Hansson, H.-C. Wiedensohler, A., Noone, K. J., Ogren, J., Hallberg, A. and Colvile, R. 1994. Hygroscopic growth of aerosol particles and its influence on nucleation savenging in cloud: experimental results from Kleiner Feldberg. *J. Atmospheric Chem.* **19**, 129–152.

Timmermans, J. 1960. *The physico-chemical constants of binary systems* vol. 4. Interscience, New York.

Twomey, S. 1977. The influence of pollution on the shortwave albedo of clouds. *J. Atmos. Sci.* **34**, 1149–1152.

Twomey, S. 1991. Aerosols, clouds and radiation. *Atmospheric Environment* **25A**, 2435–2442.

Vesala, T. and Kulmala, M. 1993. Comparison of uncoupled, film theoretical and exact solutions for binary droplet evaporation and condensation. *Physica A* **192**, 107–123.

Wagner, P. E. (1985). A constant-angle mie scattering method (CAMS) for investigation of particle formation processes. *J. Colloid Interface Sci.* **105**, 456–467.

Zhang, X. Q., McMurry, P. H., Hering, S. V. and Casuccio, G. S. 1993. Mixing characteristics and water content of submicron aerosols measured in Los Angles and at the Grand Canyon. *Atm. Env.* **27A**, 1593–1608.